Detection of the pulp-froth interface using the ultrasound transit time technique

Richter, T.; Heitkam, S.; Odenbach, S.; Eckert, K.;

Originally published:

October 2020

Minerals Engineering 160(2021), 106679

DOI: https://doi.org/10.1016/j.mineng.2020.106679

Perma-Link to Publication Repository of HZDR:

https://www.hzdr.de/publications/Publ-29111

Detection of the pulp-froth interface using the ultrasound transit time technique

T. Richter[a,*], S. Heitkam[a,b], S. Odenbach[c], K. Eckert[a,b]

[a] *Helmholtz-Zentrum Dresden-Rossendorf (HZDR), Institute of Fluid Dynamics, Bautzner Landstrasse 400, 01328 Dresden, Germany*
E-mail: Thomas.Richter@hzdr.de
[b] *Technische Universität Dresden, Institute of Process Engineering and Environmental Engineering, 01062 Dresden, Germany*
E-mail: Kerstin.Eckert@tu-dresden.de
[c] *Technische Universität Dresden, Institute of Mechatronic Engineering, Chair of Magnetofluiddynamics, Measuring and Automation Technology, 01062 Dresden, Germany*

Abstract

The height of the pulp-froth interface in a flotation cell is an important parameter in froth flotation processes which needs to be controlled in situ. For this purpose, we introduce the ultrasound transit time technique (UTTT), a new and non-invasive means of detecting and measuring the height of this interface. Based on measurements, the method is evaluated for a pulp-air and a pulp-froth interface in a lab-scale setup. The accuracy is found to equal 2%.

Keywords: lab-scale flotation; level height detection; pulp-froth interface; ultrasound transit time technique

1. Introduction

Froth flotation is an important process in mining to extract valuable mineral particles from valueless gangue particles. A number of parameters are relevant for controlling froth flotation processes, including the bubble size distribution, the bubble surface area flux, and the formation of the pulp-froth interface [1, 2, 3]. The height of the pulp-froth interface in a flotation cell, especially, is a major parameter when it comes

*Corresponding author

to controlling the grade of the concentrate.

To detect the pulp-froth interface, pressure sensors, conductivity and capacitance probes, microwave radar, ultrasound transmitters and optical measurements have been employed [4, 5, 6]. Pressure sensors cannot be applied directly to the pulp, but they can be attached on top of side tubes. This configuration enables the interface to be continuously detected over a certain range [4]. Capacitance probes use the change in the dielectric constant from air to liquid. They can either be applied directly to the pulp or attached to a side tube [4]. Conductivity probes rely on the shift in the electric conductivity from pulp to froth. A number of probes can be installed equidistantly along a tube and the change in the interface height thus measured discretely, elicited by the space in between the probes [7, 8]. The signals from microwave radar and ultrasound transmitters are sent through the pulp and are reflected by a floating object at the pulp-froth interface [6]. The accuracy of the ultrasound transmitters is limited by the assumption that the froth and pulp density are uniform [8]. Another approach to apply ultrasound is to measure from the top of a flotation cell. Here, the transducer, positioned above the froth, emits pulses with a frequency in the kHz range, which are reflected by a float supported on the top of the froth [9]. The interface can be detected visually if optical access to the cell can be enabled [5].

For use in lab-scale flotation cells, capacitance and pressure probes, as well as the float techniques, are able to detect the position of the pulp-froth interface to within ± 1 mm [4]. These methods are more invasive, which could be disadvantageous in some applications where aggressive liquids are utilized.

The present work focuses on the application of a noninvasive ultrasound technique, known as the ultrasound transit time technique (UTTT), for detecting the pulp-froth interface through the bottom of the tank, a method which has not been applied before. UTTT originates from non-destructive material testing, and was developed in particular in connection with advanced flowmeters ([10, 11]). It measures the time of flight t_f for a sound pulse to travel from an ultrasound transducer to a certain reflecting object and back to the transducer. Knowing the speed of sound c, this yields the distance between

the transducer and the reflecting object s.

$$s = c\frac{t_f}{2}. \tag{1}$$

UTTT was utilized in a multi-phase flow to detect bubbles and to measure their trajectories and diameters, or the tilt angles of ellipsoidal bubbles in water and in liquid metals. A detailed comparison with other techniques, such as optical measurements and X-ray radiography, has demonstrated the accuracy of UTTT for measurements in multiphase flows [12, 13, 14].

The motivation for the present study is a quantitative evaluation of the capability of UTTT to detect the pulp-froth interface. For that purpose, we apply UTTT with different sound frequencies to (1) pure water with different filling levels and stirring rates, (2) stirred particle suspensions with different particle fractions, and (3) stirred particle suspensions with different particle fractions and added frother. The speed of sound for each measurement is determined by simultaneously measuring the time of flight between a reference transducer and an artificial reflection target at a known distance h_T. The accuracy of the level measured is assessed by comparison with the level as measured with a ruler.

2. Experimental setup

A sketch of the setup is shown in Fig. 1. The tank was made of acrylic glass and had an inner diameter of $D = 100$ mm and a height of $H = 150$ mm. Four baffles with a thickness of $D/10 = 10$ mm were placed equidistantly at the circumference of the tank to reduce waves on the interface. A porous tube charged with compressed air was positioned close to the bottom of the tank to generate bubbles distributed along the circumference of the tank. A mass fraction of up to $\phi = 4.7\%$ of quartz particles with $d_p = 165$ μm mean diameter were added to the tank. An impeller with three blades with a diameter of $D_{im} = 45$ mm was placed at a distance of $C = 10$ mm above the bottom of the tank. The minimum impeller speed N_{zw} that prevents the sedimentation of the quartz particles is defined by the Zwietering correlation:

$$N_{zw} = S\,\nu^{0.1}\left[\frac{g\,(\rho_s - \rho_l)}{\rho_l}\right]^{0.45}\phi^{0.13} d_p^{0.2} D_{im}^{-0.85} \tag{2}$$

where ν is the kinematic viscosity of the liquid, ρ_s and ρ_l are the densities of the solid and liquid fraction respectively, ϕ is the mass fraction of the particles and S is the Zwietering constant for the impeller [15]. A correlation for a three-bladed axial impeller is given by [16]:

$$S = 8.17\left(\frac{C}{D}\right)^{0.329}\left(\frac{h}{D}\right)^{-0.244} \approx 3.8\,. \tag{3}$$

With this value and a maximum $m_{Q.r}$ of 4.76%, a critical impeller speed of $N_{zw} >$ 330 rpm is required. Due to this, the rotation rate N of the impeller was set between 300 rpm and 600 rpm.

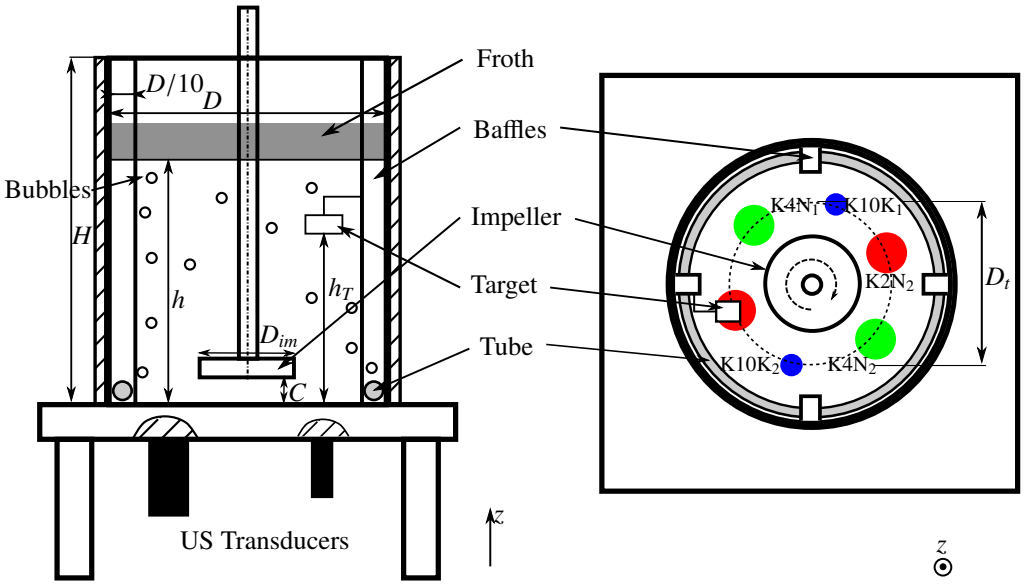

Figure 1: Schematic diagram of the experimental setup; top and side view. The gray box indicates the froth region.

The measuring principle of UTTT is based on single ultrasonic pulses emitted by a transducer and is described in detail in [17]. The transducer is acoustically coupled to a tank wall and emits wave packets of up to 5 wave trains with a frequency f, which are repeated with a pulse repetition frequency f_p in the kHz range. These pulses are reflected by any discontinuity in the acoustic impedance. In the present case, these are the interface between the tank wall and the pulp, between the pulp and the air

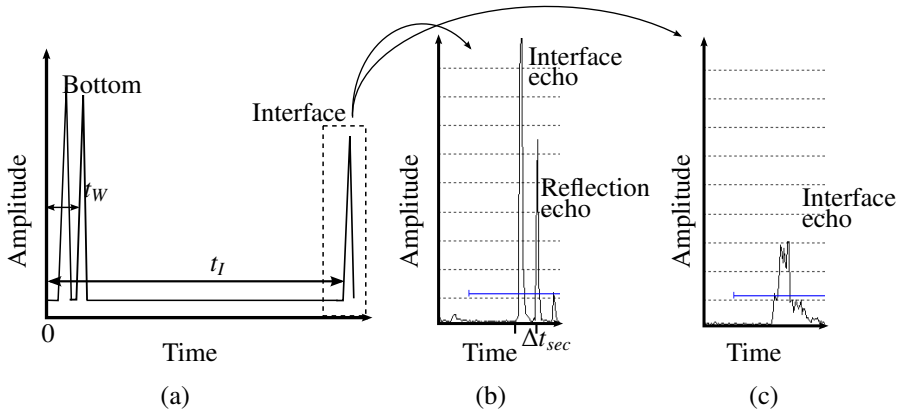

Figure 2: (a) Schematic amplitude diagram illustrating the echo signal from the interface between the bottom of the tank and the pulp, detected at a time t_W, and from the pulp-air or pulp-froth interface, detected at t_I. (b) Detail of the amplitude diagram showing the echo signal from the pulp-air interface. The secondary peaks represent multiple reflections in the bottom wall of the tank. (c) Detail of the amplitude diagram showing the signal of the interface for the pulp-froth case.

and between the pulp and the froth. The echo is recorded by the same transducer, yielding the echo intensity over time. Fig. 2 (a) shows a typical amplitude diagram. The transit time is the elapsed time between the transmission of the pulse and the time at which the rising flank of the echo is detected. Figs. 2 (b) and (c) show a typical amplitude diagram of the echo from a pulp-air and pulp-froth interface, respectively. The secondary peaks after the first one in Fig. 2 (b) are caused by the pulse being reflected multiple times from the bottom wall of the tank. The measured time shift

Table 1: Types and parameters of the employed transducers: diameters d_t, emission frequency f, corresponding wavelength λ in pure water and the parameter ka, given by the product of the wave number $k = 2\pi/\lambda$ and the particle diameter a. In the transducer nomenclature, e.g. K2N, K refers to the type of the transducer, 2 (MHz) to the frequency and N to the size (d_t).

Type	d_t [mm]	f [MHz]	λ [μm]	ka [−]
K2N	10	2	742	1.4
K4N	10	4	371	2.8
K10K	5	10	148.4	7.0

$\Delta t_{sec} \approx 4.35\ \mu$s between two secondary peaks is twice the ratio between the thickness of the bottom plate $s_{plate} \approx 6$ mm and the speed of sound in the plate $c_{plate} \approx 2670$ m/s, according to

$$\Delta t_{sec} \approx 2\, s_{plate}/c_{plate} \approx t_W \tag{4}$$

Δt_{sec} also corresponds to the time of flight for the first echo from the wall-pulp interface t_W. Six transducers (GE Sensing & Inspection Technologies) of three different types (cf. Table 1) were attached to the outer surface of the bottom wall of the tank (cf. Fig. 1). They vary in their working frequency (2, 4 and 10 MHz). Two identical transducers $K2N_i$ and $K4N_i$ are used for the lower frequencies 2 and 4 MHz. The transducers form a circle with $D_t = 65$ mm diameter, protruding beyond the impeller by 10 mm, see Fig. 1 (b). Opposing transducers are of the same type, meaning that their combined measurement cancels out errors caused by the tank tilting. Each transducer sends a pulse and receives the corresponding echo to measure the target quantity, namely the distance h from the bottom of the tank to the pulp-froth interface,

$$h \;=\; c \cdot \frac{t_I - t_W}{2}. \tag{5}$$

where c is the speed of sound in the pulp, t_I the transit time from the transducer to the interface and back and t_W the transit time to the wall-pulp interface and back (cf. Fig. 2 (a)). Determining h via Eq. (5) requires knowledge of c, which depends on the composition of the pulp.

The speed of sound c in the pulp can be calculated using the approach developed by [18] for small ka (viscous regime) and [19] for large ka (inertial regime). In the present case, the parameter ka, given by the product of the wave number $k = 2\pi/\lambda$ and the particle diameter $a = d_p$, is higher than 1, which falls into the inertial regime. For high parameters of $ka \gg 1$, the particles are large compared to the wavelength and the sound scatters geometrically [20], which is particularly the case for the K10K transducers in Table 1. The corresponding equation:

$$c \;=\; \sqrt{\frac{\bar{K}\left[\frac{1-\varepsilon}{2} + \frac{(1-\varepsilon)\rho^*}{\rho_l}\right]}{\frac{1-\varepsilon}{2}\bar{\rho} + (1-\varepsilon)\rho_s}} \tag{6}$$

with

$$\frac{1}{\bar{K}} = \frac{\varepsilon}{K_s} + \frac{1-\varepsilon}{K_l}\,, \tag{7}$$

$$\bar{\rho} = \varepsilon\rho_s + (1-\varepsilon)\rho_l \tag{8}$$

and

$$\rho^* = (1-\varepsilon)\rho_s + \varepsilon\rho_l\,, \tag{9}$$

yields a value of 1480 m/s when using a liquid fraction $\varepsilon = 0$. With the given height of the level, approximately 100 mm, this yields a transit time of $t_I = 134.8\ \mu$s, which is detected well by the UTTT system, which possesses a temporal resolution of $\sigma_t = 0.03\ \mu$s, yielding an uncertainty of 0.02 %. However, it is difficult to find exact values for K and ρ for both the solid and the liquid fraction. Furthermore, the void fraction in the form of gas bubbles, which is not yet considered in Eq. 9, influences the speed of sound. To obtain reliable values for c, this quantity is measured directly, parallel to the level measurements, via the transit time t_T to an artificial target placed at a defined height h_T above the transducer $K2N_1$:

$$c = \frac{2 \cdot h_T}{t_T - t_W}\,. \tag{10}$$

Eq. 5 combined with Eq. 10 leads to:

$$h = h_T \cdot \frac{t_I - t_W}{t_T - t_W}\,. \tag{11}$$

The uncertainty regarding the height measurements is accessed by the error Δh, referring to the difference between h, as measured by UTTT and the total filling height, given by $h_{tot} = h_{aq} + h_q$, i.e.,

$$\Delta h = h - h_{tot} = h - \left(h_{aq} + h_q\right). \tag{12}$$

h_{tot} takes into account the filling level of the pure water h_{aq}, measured with a ruler, and the additional height due to the addition of quartz particles h_q. The latter is calculated via the mass m_q and the density ρ_q of the added particles and the cross section A of the tank:

$$h_q = \frac{m_Q}{\rho_Q A}\,. \tag{13}$$

The relative error r_h of the measured height is calculated by:

$$r_h = \frac{\Delta h}{h_{tot}} . \tag{14}$$

Negative values of Δh and r_h indicate that the filling height is underestimated.

The tank was filled with a volume of 800 ml of tap water up to a height of $h_{aq} = (108.2 \pm 0.5)$ mm. The target was placed at a height of $h_T = (71 \pm 0.5)$ mm above the transducer $K2N_1$. The transducers $K4N_1$, $K10K_1$, $K2N_2$, $K4N_2$ and $K10K_2$ were used to measure h.

Different mass fractions of hydrophobic quartz particles were added to the tank (cf. Table 3). These were hydrophobized using the surfactant CTAB (Sigma Aldrich, BioXtra $\geq$ 99%). 18.22 mg of CTAB was added to 50 g of quartz sand and mixed with 50 ml of water. Afterward, the sand particles were filtered and dried. A German dish-washing soap (FIT) was used as a frother. This led to a very stable froth. The air flow through the porous tube was enabled during all the measurements. In the cases of pure water-air (1) and pulp-air (2), the air flow rate was set to $Q_g = 1$ cm^3/s, resulting in a mean bubble size of approximately 3 mm as determined from camera pictures. In the case of pulp-froth (3), the air flow rate was reduced to $Q_g = 0.5$ cm^3/s (mean bubble size of $1.0 - 2.0$ mm) to prevent the froth from overflowing.

Table 2: Material parameters of water at $\vartheta = 20°$C and of quartz: density ρ, sound velocity c and bulk modulus K.

-	ρ [kg/m^3]	c[m/s]	K[GPa]
water	998	1484	2.2
quartz	2564.1	6050	97

Table 3: Mass m_Q, mass fraction ϕ of the quartz particles ($d_p = 165\mu$m) and additional height h_q due to added quartz volume.

m_Q [g]	0.5	1.0	2.0	4.0	8.0	20.0	40.0
ϕ [%]	0.062	0.124	0.248	0.496	0.992	2.44	4.76
h_Q [mm]	0.025	0.05	0.1	0.2	0.4	1.0	2.0

3. Results

3.1. Pure water

The first measurements were made in pure water at different filling heights h_{aq} without stirring, to analyze the linearity of the measurements. Fig. 3 depicts the correlation between the measured height h and the filling height h_{aq} and Fig. 4 the relative error averaged over 10^4 measurement values and over pairs of the same transducer type (K2N, K4N and K10K). The measured height h correlates linearly with h_{aq} and underestimates the filling level by less than 2 %. For low filling levels, the speed of sound gained at the height h_3 was used to calculate the heights h_1 and h_2 since the artificial target could only be submerged at $h \leq h_3$.

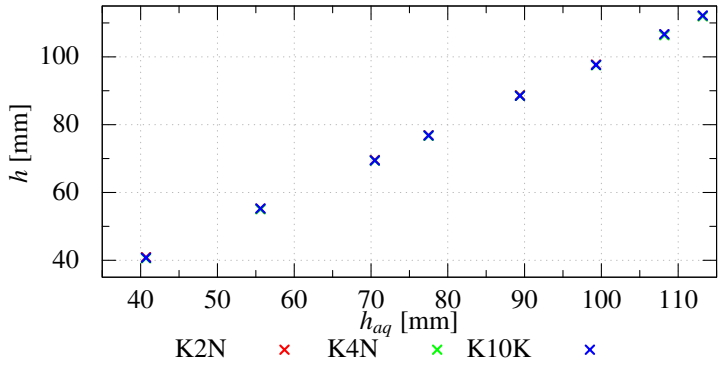

Figure 3: Measured height h plotted over the filling height h_{aq} of the interface for $N = 0$ rpm.

Now, the impeller is set to different rotation rates in order to test the influence of the stirring motion on the measurement. Fig. 5 plots the interface height h measured by UTTT versus the rotation rates at an unchanged filling level of $h_{aq} = 108$ mm. Each transducer carries out 10 individual transit time measurements. Fig. 5 reports the mean values and the corresponding standard deviations.

When the rotation rate is increased, the mean value of all measurements equals approximately 106.75 mm and is independent of the rotation rate. The scatter of the mean values of the various transducers, placed at different positions on the bottom of the tank (cf. Fig. 1), and also the corresponding standard deviation, increase along with the rotation rate. To a large extent, this increase is the result of the water surface level

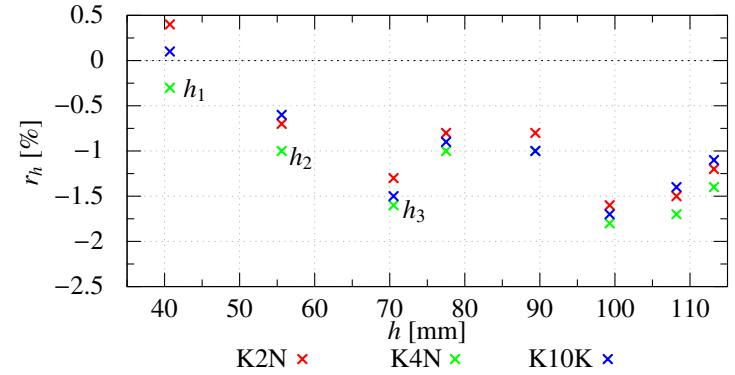

Figure 4: Relative error r_h for different heights of the interface for $N = 0$ rpm.

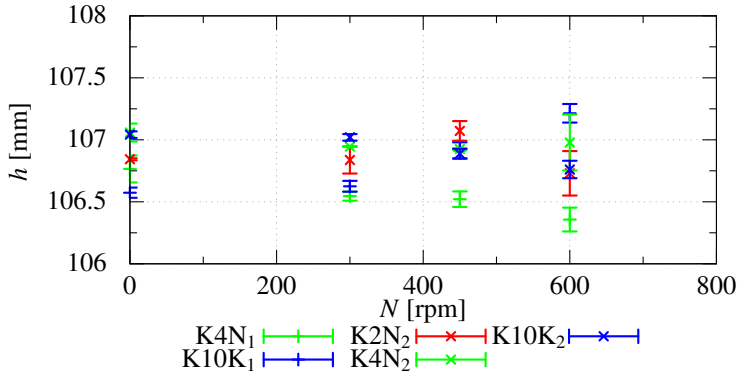

Figure 5: Measured interface height h in pure water at a filling level $h_{aq} = 108.2$mm for different impeller rotation rates N.

fluctuating due to the stirring. The recording time for 10^4 individual signals equals 10 s. This is in the order of the frequency of typical surface waves in the tank. Consequently, the mean value is also influenced by surface waves.

Fig. 6 shows pictures of the surface waves. Figs. 6 (a) and (b) are compared to underline the fact that stirring did not generate a swirl changing the average height of the interface. Fig. 6 (b) shows that the interface exhibited surface waves with an amplitude of approximately 2 mm. Fig. 6 (c) visualizes the unsteady wave pattern. No standing waves were observed.

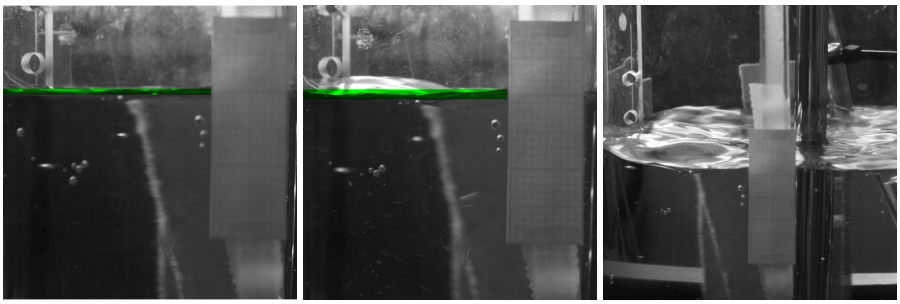

(a) (b) (c)

Figure 6: Interface level (a) for the impeller when stopped and (b) at $N = 600$ rpm. No change in the average level was detectable when the rotation rate was increased (cf. green line in the pictures). However, an unsteady pattern structure of surface waves was visible on the interface at $N = 600$ rpm (c).

3.2. Particle suspension

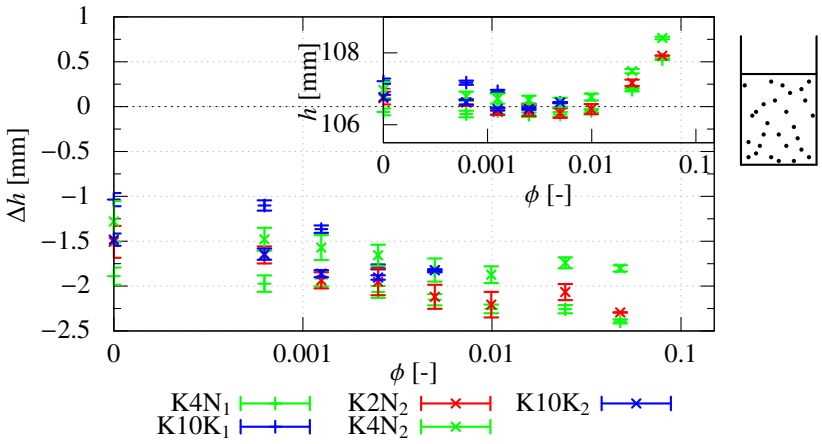

Figure 7: Heights of the pulp-air interface h measured by UTTT together with their absolute errors Δh versus solid fraction for all transducers at $N = 600$ rpm.

Next, hydrophobized quartz particles are added to the water with increasing solid fractions ϕ leading to a small stepwise increase in the liquid level in the tank. Fig. 7 shows that this increase is reflected by the UTTT measurements of the absolute height h. The absolute measurement error Δh increases slightly to 2 mm at the highest solid fraction $\phi = 0.047$ and the measured interface height h for all transducers at

N = 600 rpm. Hence, the particle fraction does not affect the level detection strongly as long as ultrasound frequencies (2 and 4 MHz) are used at which the wavelength (cf. Table 1) is significantly larger than the particle diameter d_p = 165 μm. This is no longer valid for the measurement with the highest frequency (10MHz), which loses validity above a solid fraction of 1 % due to strong scattering of the ultrasound waves at the suspended particles.

The variation in the mean values of h and the temporal fluctuation were slightly reduced by the addition of particles. This could be due to the increased effective viscosity of the pulp and thus the decreased amplitude of the surface waves.

3.3. Particle suspension with frother

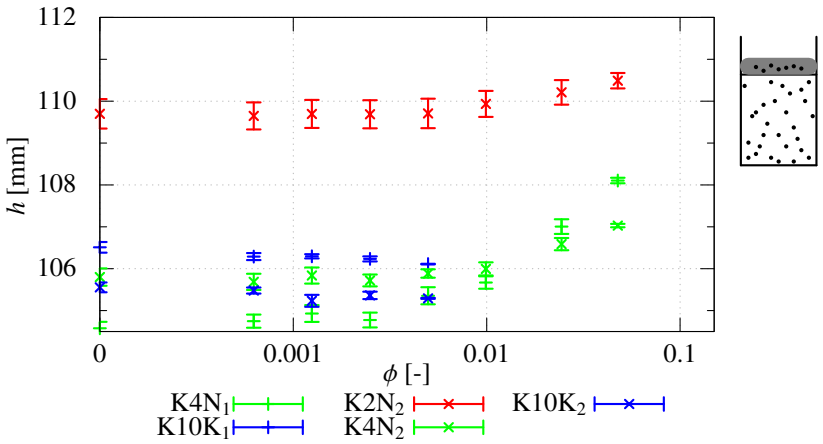

Figure 8: Interface heights h for all transducers for the pulp-froth application at N = 600 rpm.

Finally, frother is added to the system in order to generate a layer of stable froth that is approximately 25 mm thick on top of the pulp and to test the measurement approach on the pulp-froth interface. Figs. 8 and 9 show the measured interface heights and corresponding errors, respectively. The interface can be detected with an uncertainty of ± 2.5 %. Detection can be optimized with the 4 MHz transducers. Again, the transducers with the highest frequency (K10K) are not applicable in the case of a high solid fraction for the reason explained above. The transducer with the lowest frequency

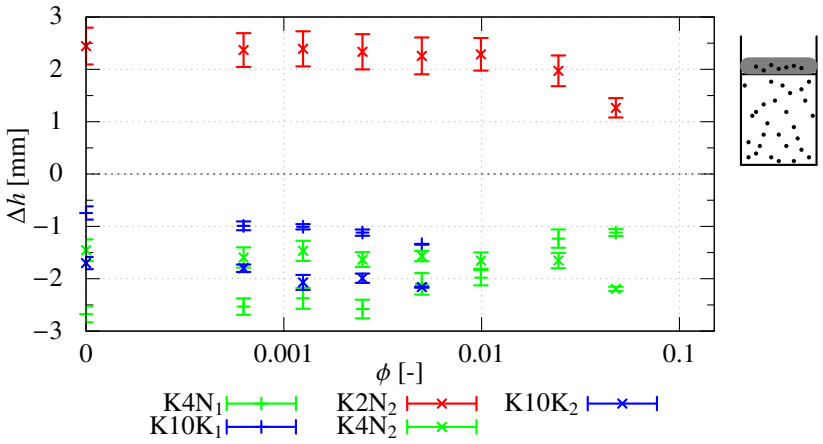

Figure 9: Absolute error Δh for all transducers for the pulp-froth application at $N = 600$ rpm.

(K2N, 2MHz) yields an interface position which is about 4.5mm higher than the other transducers. There are two possible explanations for this behavior: (i) The lower ultrasound frequency partly penetrates the froth. Thus, the echo is shifted towards larger transit times. At higher solid fractions this trend is counteracted by hydrophobized particles being entrained into the froth, which again reduces the penetration depth of the signal. (ii) Froth damps surface waves on the pulp-froth interface [21], leading to the formation of standing waves on the interface due to the stirring. Consequently, in front of the baffles the stagnation of the rotary movement generates increased pressure and thus leads the interface to shift upward (cf. Fig. 10). Since transducers K2N are placed before the baffles (cf. Fig. 1) this might result in an overestimation of the level. Again, this effect is reduced when the particle fraction is higher due to increased effective viscosity.

3.4. Speed of sound in the suspension

The speed of sound c in the cases of pulp-air and pulp-froth, which was constantly recorded by the transducer $K2N_1$, is plotted in Fig. 11. The theoretical relation [19] for c (Eq. 6) is computed to evaluate the trends of the measured c. For the speed of sound in pure water, $c(\phi = 0)$, the measured value was used for better comparability. The

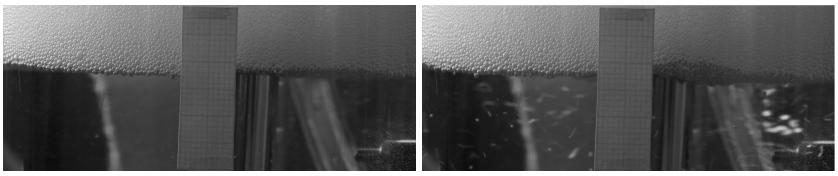

(a) (b)

Figure 10: Water-froth interface without stirring (a) and with stirring (N = 600 rpm) in (b). The interface was deformed additionally by the froth structure, especially in front of the baffles. This deformation did not totally subside after the impeller was stopped, due to the finite yield stress of froth.

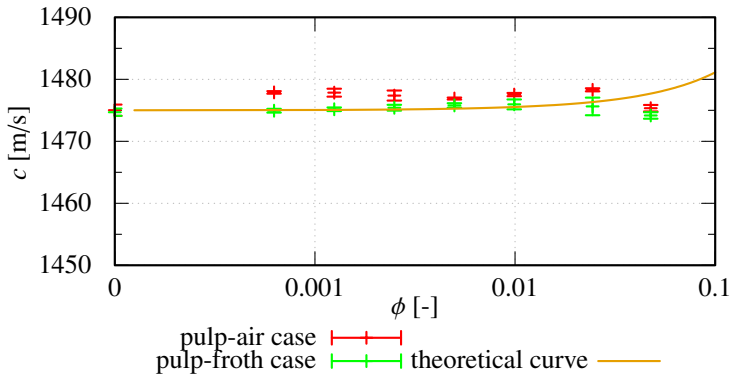

Figure 11: Sound velocity c for the pulp-air, the pulp-froth application and the theoretical relation for the sound velocity in a suspension for $ka \geq 1$ [19].

gas phase is negligible, since no gas is dispersed and only few bubbles rise in the pulp, which are in any case too large to have any distinct impact on the speed of sound. The measured values fit well to the theoretical relation, which is reasonable as all $ka \geq 1$.

4. Discussion

The interface heights h can be measured robustly, with an uncertainty of less than 2 %. This uncertainty could be elicited by a deviation in the target height h_T for the calculation of the speed of sound c. A deviation of ±0.5 mm for h_T and an uncertainty of ±0.02 μs for the transit times t_T and t_W could lead to a theoretical relative error for c of $r_c = \pm 1.12$ %. This results in a theoretical relative error $r_h = \pm 1.54$ %, or a theoretical absolute error $\Delta h = \pm 1.67$ mm, respectively. Nonetheless, the direct

acquisition of c offers the advantage that changes in the composition of the pulp and in the temperature can be captured well.

The interface height decreased as the particle content increased in cases (2) and (3), as can be seen in Figs. 7 and 9. This reduction amounted to approximately $0.7 - 0.8$ mm ($r = 0.7\%$), which correlates to a fluid volume of $5 - 6$ ml. This reduction in the level is associated with both a low level of evaporation and a small discharge of water related to the experimental routines. For instance, thin water films remained both at the ruler used to check the interface, and at the stirring spatula used to insert the quartz and to remove bubbles below the target.

Taking this systematic error into account, the current deviation in the filling height of approximately 2.2 mm can be reduced to approach the desired set point of ± 1 mm for lab-scale operation. This is also supported by the fact that the variation in the interface height due to the particle insertion h_q, which is comparable to a set point change, was covered very well (cf. Figs. 7 and 8). In summary, UTTT can be applied to detect the level in a lab-scale flotation setup, but the deviation from the filling height has to be considered and corrected.

5. Conclusions

This work shows that UTTT can be used to detect the height of the pulp-air interface and the pulp-froth interface in a lab-scale flotation cell. The measured height of the interface differed from the total filling height by up to 2% i the case of pulp-air, and 2.5% in the case of pulp-froth. The sound velocity of the pulp was also detected, and changed slightly depending on the composition of the pulp.

Acknowledgments

We would like to thank Peggy Jähnigen for preparing the hydrophobic particles, Andre Kupka for measuring the size and Michael Knobel for measuring the density of the quartz particles.

References

[1] J. Yianatos, F. Henríquez, Boundary conditions for gas rate and bubble size at the pulp–froth interface in flotation equipment, Minerals engineering 20 (6) (2007) 625–628.

[2] L. Vinnett, F. Contreras, J. Yianatos, Bubble size analysis and boundary conditions for automatic control of industrial flotation cells, IFAC Proceedings Volumes 42 (2009) 161–166.

[3] J. Leiva, L. Vinnett, F. Contreras, J. Yianatos, Estimation of the actual bubble surface area flux in flotation, Minerals Engineering 23 (11-13) (2010) 888–894.

[4] J. Hamilton, P. Guy, Pulp level control for flotationoptions and a csiro laboratory perspective, Minerals engineering 14 (1) (2001) 77–86.

[5] P. Jampana, S. Chitralekha, S. L. Shah, Image-based level measurement in flotation cells using particle filters, IFAC Proceedings Volumes 42 (23) (2009) 116–121.

[6] B. Shean, J. Cilliers, A review of froth flotation control, International Journal of Mineral Processing 100 (3-4) (2011) 57–71.

[7] J. Van Deventer, D. Feng, A. Burger, The use of bubble loads to interpret transport phenomena at the pulp–froth interface in a flotation column, Chemical Engineering Science 56 (21-22) (2001) 6313–6319.

[8] M. Maldonado, A. Desbiens, R. Del Villar, An update on the estimation of the froth depth using conductivity measurements, Minerals Engineering 21 (12-14) (2008) 856–860.

[9] M. D. Bishop, Froth level measurement (dec 1991).

[10] P. I. Moore, G. J. Brown, B. P. Stimpson, Ultrasonic transit-time flowmeters modelled with theoretical velocity profiles: methodology, Measurement Science and Technology 11 (12) (2000) 1802.

[11] D. V. Mahadeva, R. C. Baker, J. Woodhouse, Further studies of the accuracy of clamp-on transit-time ultrasonic flowmeters for liquids, Instrumentation and Measurement, IEEE Transactions on 58 (5) (2009) 1602–1609.

[12] T. Richter, K. Eckert, X. Yang, S. Odenbach, Measuring the diameter of rising gas bubbles by means of the ultrasound transit time technique, Nuclear Engineering and Design 291 (2015) 64–70.

[13] T. Richter, O. Keplinger, E. Strumpf, T. Wondrak, K. Eckert, S. Eckert, S. Odenbach, Measurements of the diameter of rising gas bubbles by means of the ultrasound transit time technique, Magnetohydrodynamics 53 (2) (2017) 383–392.

[14] T. Richter, O. Keplinger, N. Shevchenko, T. Wondrak, K. Eckert, S. Eckert, S. Odenbach, Single bubble rise in gainsn in a horizontal magnetic field, International Journal of Multiphase Flow 104 (2018) 32–41.

[15] T. N. Zwietering, Suspending of solid particles in liquid by agitators, Chemical Engineering Science 8 (3-4) (1958) 244–253.

[16] C. Devarajulu, M. Loganathan, Effect of impeller clearance and liquid level on critical impeller speed in an agitated vessel using different axial and radial impellers., Journal of Applied Fluid Mechanics 9 (6).

[17] A. Andruszkiewicz, K. Eckert, S. Eckert, S. Odenbach, Gas bubble detection in liquid metals by means of the ultrasound transit-time-technique, The European Physical Journal Special Topics 220 (1) (2013) 53–62.

[18] R. Urick, A sound velocity method for determining the compressibility of finely divided substances, Journal of Applied Physics 18 (11) (1947) 983–987.

[19] C. Atkinson, H. Kytömaa, Acoustic wave speed and attenuation in suspensions, International Journal of multiphase flow 18 (4) (1992) 577–592.

[20] H. K. Kytömaa, Theory of sound propagation in suspensions: a guide to particle size and concentration characterization, Powder Technology 82 (1) (1995) 115–121.

[21] A. Sauret, F. Boulogne, J. Cappello, E. Dressaire, H. A. Stone, Damping of liquid sloshing by foams, Physics of Fluids 27 (2) (2015) 022103.